Int. J. Electrochem. Sci., 13 **(2018)** 3246 – 3256, doi: 10.20964/2018.04.33

International Journal of
ELECTROCHEMICAL
SCIENCE
www.electrochemsci.org

Short Communication

Corrosion Behaviour of 316L Stainless Steel in Boric Acid Solutions

Shenghan Zhang, Quan Lu, Yunfei Xu, Kuan He, Kexin Liang[*]*, Yu Tan*

Department of Environment Science and Engineering, North China Electric Power University, Yonghua North Street 619#, Baoding 071003, China.
[*]E-mail: kexin91802@163.com

Received: 30 September 2017 / *Accepted:* 25 January 2018 / *Published:* 6 March 2018

The corrosion behaviour of stainless steel 316L in boric acid solutions to simulate the environment in the primary circuit of a pressurized water reactor was investigated by electrochemistry, the weight loss method, scanning electron microscopy, and X-ray diffraction. The results indicated that during a 7 day corrosion process at temperatures ranging from 50 to 185°C, the stainless steel 316L had very low corrosion rates. The corrosion of a passive protection layer on the surface were investigated. The electrochemistry results showed that the open circuit potential of the samples increased as the corrosion process developed, and at high concentrations of boric acid, a more positive open circuit potential was observed. The Nyquist plots displayed a shrinking semi-circle as the corrosion time increased. Bode diagrams indicated the time constant during the corrosion process. The morphology results suggested that the metal oxides changed from large deposits to small scaly deposits as the boric acid concentration increased. X-ray diffraction analysis suggested that the oxide layer on stainless steel 316L after corrosion had the same composition even when different concentrations of boric acid were used. These results grant insight into the corrosion behaviour of 316L stainless steel in boric acid solutions during the operation of pressurized water reactors.

Keywords: Stainless steel 316L; Boric acid; Corrosion; Electrochemical behaviour

1. INTRODUCTION

Boric acid, which is used as a neutron absorber in the primary circuit of many pressurized water reactor (PWR) plants, may also cause corrosion problems at certain concentrations[1-2] due to poor water flow. In PWRs, several components are made of high alloy steels. Such materials are in direct contact with the PWR primary circuit environment and should form a corrosion resistant layer during exposure to the primary water[3-6]. Under these conditions, when a boric acid solution is

concentrated at a specific location, the high alloy steels may corrode in a short time. Stainless steel 316L (SS316L) is used for the main pipeline due to its mechanical properties, ability to withstand high temperatures, and uniform resistance to corrosion. When used in a high temperature and irradiated environment with high-pressure water in a PWR, the stainless steel must ensure structural integrity and have a lower corrosion rate to reduce the oxidation process in the reactor core activation and in the radiation field outside the core. It has been reported that pitting corrosion and stress corrosion cracking (SCC) are related to the oxide films on stainless steel [7-8]. The complexities of the factors that affect the passivation of stainless steel are not only reflected in the microstructure but also in environmental effects [9-10]. In the past, researchers have paid more attention to the damaging effect of the Cl^- environment on the passivation behaviour [11-12]. The pitting potential was simply used as a characteristic parameter to evaluate the stability of the passivation film. Uemura [13] and Dacunhabelo [14] studied the structure of passivation films on SS316L using Mott-Schottky plots and Raman spectroscopy. They noted that the passive film was a multi-layer structure with an outer layer composed mainly of iron oxide and an inner layer composed mainly of chromium oxide. The corrosion behaviour of stainless steel in boric acid solution should be given more attention because storage grids for spent fuel components are also composed of stainless steel operating within a boric acid and water environment[15-16]. The study of corrosion behaviour is important for understanding the structural effects of fuel components.

In this work, the effects of the temperature in conjunction with the composition of the solution on the corrosion and electrochemical behaviour of SS316L in boric acid solutions at temperatures ranging from 50 to 185°C were studied by weight loss measurements, electrochemical measurements and morphology observations. Investigation into the corrosion properties of stainless steel in a boric acid solution will be helpful for understanding the mechanism affecting corrosion in a PWR environment.

2. EXPERIMENTAL

The chemical composition (wt%) of the SS316L used in this work is given in Table 1. Sections of 40×15×2 mm with a 1 mm diameter hole for hanging were employed for the corrosion weight loss measurements. The samples for the electrochemical measurements were spot-welded to copper wires for electrical contact and then mounted in epoxy with a 6 mm diameter section exposed to the test solutions. Before the measurements, the surfaces were ground mechanically with 2000 grit SiC paper and then polished with 0.3 μm Al_2O_3 powders. Additionally, ethanol and water were employed for ultrasonic cleaning.

Table 1. Chemical composition (wt%) of stainless steel 316L

Element	Si	Mn	P	Mo	Cr	Ni	C	S	Fe
Concentration (wt %)	0.6	0.8	0.013	2.28	17.14	12.58	0.014	0.0073	balance

A solution containing 1200 ppm B (counted by H_3BO_3), 2 ppm Li (LiOH) and 200 ppb Co $(CH_3COO)_2Co$), named *1200B2Li*, was used to simulate the radiation product composition of a normal PWR. A solution with 6000 ppm B, 10 ppm Li and 1000 ppb Co was named *6000B10Li*, and a solution composed of 12000 ppm B, 20 ppm Li and 2000 ppb Co was named *12000B20Li*. Additionally, deionized pure water was used as a control and was named *boric-free*. For the weight loss measurements, the samples were carefully weighed before and after the corrosion process. This measurement met the requirements of IOS standard 1845:1995. The average corrosion rates, V_{corr} ($mm.y^{-1}$), were calculated by dividing the total weight loss by the corrosion period. Before heating, the solution was kept in an autoclave with the hanging samples and was bubbled with pure nitrogen for 30 min. The samples were corroded for 7 days in the autoclave at temperatures of 50, 95, 140 and 185°C. Three parallel samples were used for each test condition.

A three-electrode system was employed to investigate the electrochemical behaviour of SS316L. The working electrode was a prepared SS316L sample, the counter electrode was a platinum plate, and the reference electrode was a saturated calomel electrode (SCE) at room temperature. Electrochemical impedance spectroscopy (EIS) plots were measured by a PARSTAT2273 electrochemical workstation. EIS measurements were conducted at open circuit potentials (OCP) in a frequency range from 1 MHz to 10 mHz at an AC amplitude of 10 mV. The EIS results were fitted by ZSimpwin3.21. The morphologies of the surface after corrosion were analysed using a field emission scanning electron microscope (FE-SEM) with energy dispersive X-ray spectroscopy (EDS, coupled with an SEM) on a Hitachi S4800 instrument. The X-ray diffraction (XRD) was used for the phase analysis at room temperature (Bruker D8) with Cu Ka radiation and a voltage of 30 kV (30 mA). The 2Θ angle range was from 30° to 90°. The obtained XRD patterns were analysed using the Jade6.0 software.

3. RESULTS AND DISCUSSION

3.1. Weight loss corrosion behaviour

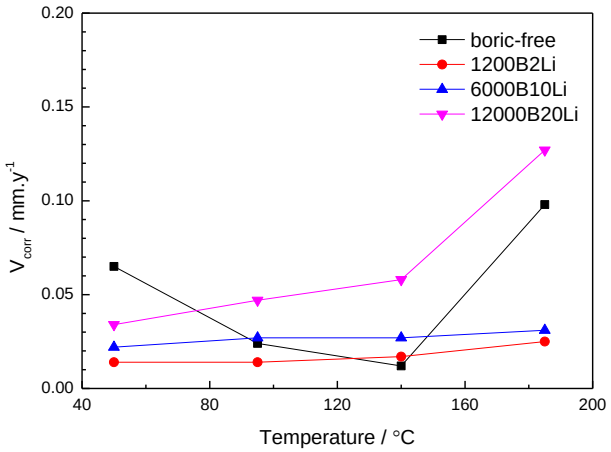

Figure 1. Corrosion rates based on the weight loss results from a 7 day immersion of SS316L in boric acid solutions at temperatures of 50, 95, 140 and 185°C.

Fig. 1 shows the resulting corrosion rates based on the weight loss method for SS316L immersed for 7 days in various boric acid solutions at different temperatures. As the samples remained shinny and bright after 7 days of the corrosion process, a rust remover was not employed in this test after the corrosion cleaning. It can be concluded that as the concentration of boric acid increased, the corrosion rate was primarily enhanced. Further, as the temperature increased, most of the corrosion rates in the boric acid solutions increased. While the boric-free data represents samples corroded in pure water, their corrosion rate was not the lowest. At 50°C, the corrosion rate of SS316 L in pure water was higher than that in any of the boric acid solutions. It may be that the boric acid and lithium hydroxide (LiOH) work as a buffer solution during the corrosion process. In contrast, in pure water, localized corrosion may cause a decrease in the pH without any buffering, and then, the low pH accelerates the corrosion rate. Regardless, the corrosion rates of SS316L in boric acid solutions from 50 to 185°C indicated a low corrosion speed according to the protective ability of stainless steel. Given this, it can be concluded SS316 L is suitable for use in the temperature range from 50 to 185°C, even in a concentrated boric acid environment.

3.2. Electrochemistry corrosion behaviours in solutions

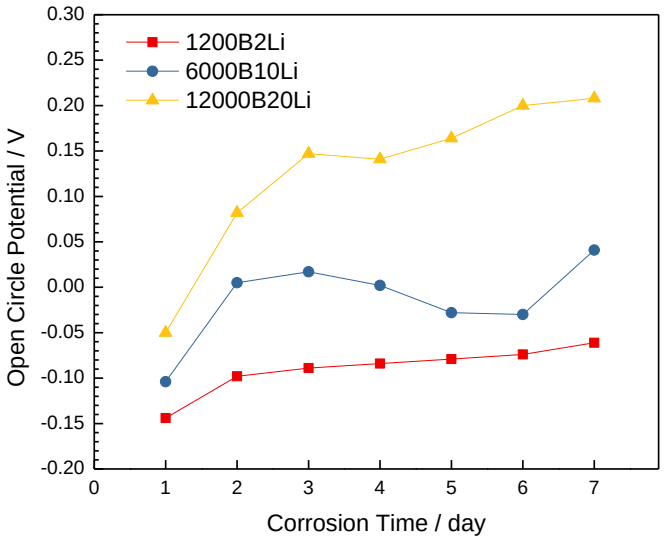

Figure 2. Open circuit potential vs. corrosion time plots of SS316 L in various boric acid solutions.

The plots of the OCP vs. corrosion time for SS316L for different boric solutions at 50°C are shown in Fig. 2. At the very beginning of this test, the OCP of SS316L immersed in different concentrations of boric acid solutions showed different OCPs. The sample in a solution with a low concentration of boric acid displayed a lower potential than the sample in a solution with a higher concentration of boric acid. During the corrosion process, the OCP slowly became more positive as time progressed regardless of the concentration of boric acid in the solution. Usually, the OCP value depends on many factors, including solution composition, concentration, temperature, film thickness,

pH and so on[17-18]. In general, for stainless steel and carbon steel, high pH solution indicated low OCP. With the extension of the corrosion time, the OCP increased, possibly with the prolongation of the corrosion product film thickening.

The EIS Nyquist and Bode diagrams for SS316L measured at open circuit potential (OCP) in boric solutions at 50°C are shown in Fig. 3. The Nyquist plots of SS316L displayed one capacitive semicircle after the initial corrosion, which became approximately linear after 2 days. The impedance modulus is generally proportional to the corrosion resistance of a metal. This means that the SS316L corrosion increased with time because the Nyquist diagrams shrank as the corrosion process developed. The Bode diagrams in Fig.3 indicated two time constants with a single corrosion reaction on the surface of SS316L. At the very beginning of the test involving the 1200 ppm boric acid solution, the low frequency impedance modulus, $|Z|_{0.01Hz}$, was higher than 10^5 Ω.cm^2 with a phase angle of 60°, which indicated a normal anti-corrosion property. As the time increased, the $|Z|_{0.01Hz}$ increased slowly, and the phase angle increased to 70~80°. When the sample of SS316L was exposed to a 6000 ppm boric acid solution, the bode diagrams vs. corrosion time exhibited the same trend with a slightly higher $|Z|_{0.01Hz}$ and phase angle. When the sample was corroded in a much higher concentration boric acid solution, the primary $|Z|_{0.01Hz}$ indicated a low value of approximately 10^2 Ω.cm^2 with a nearly 0° phase angle.

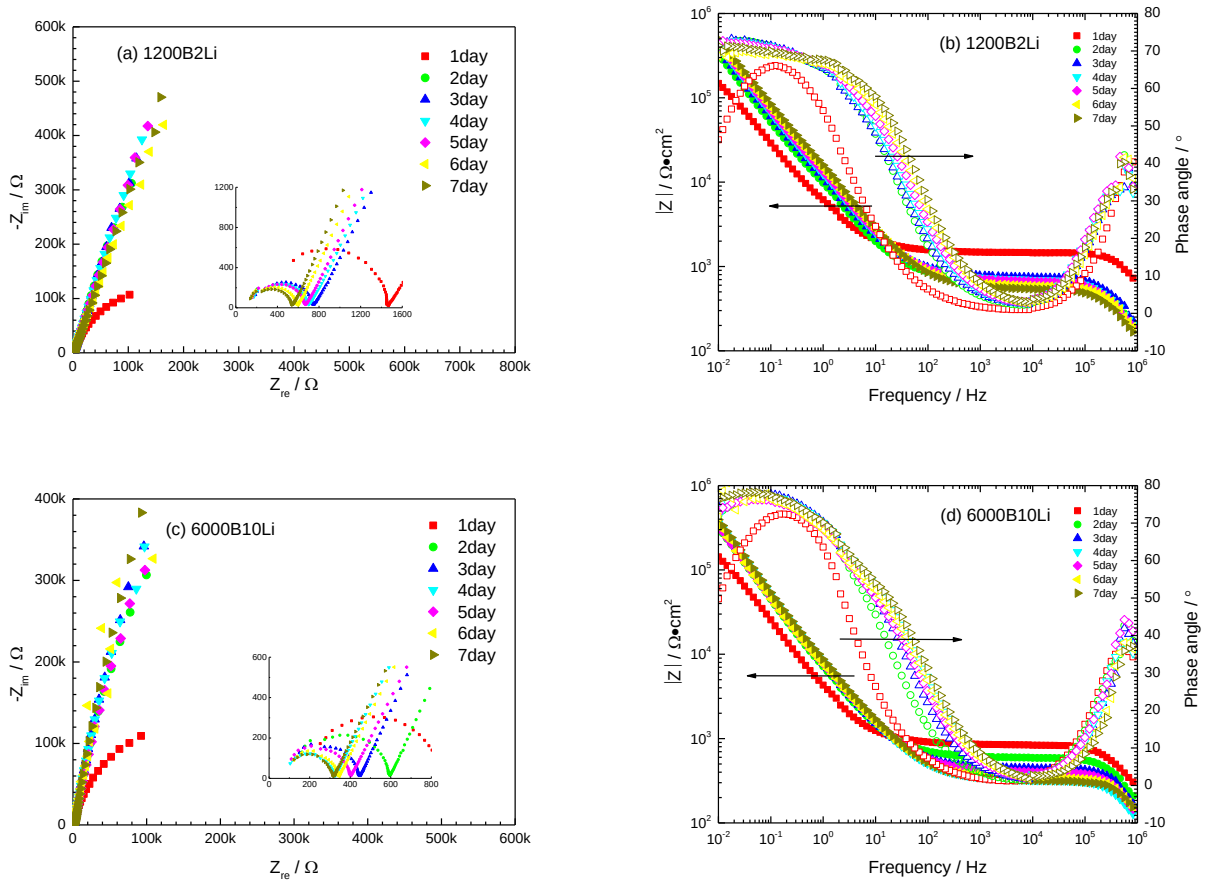

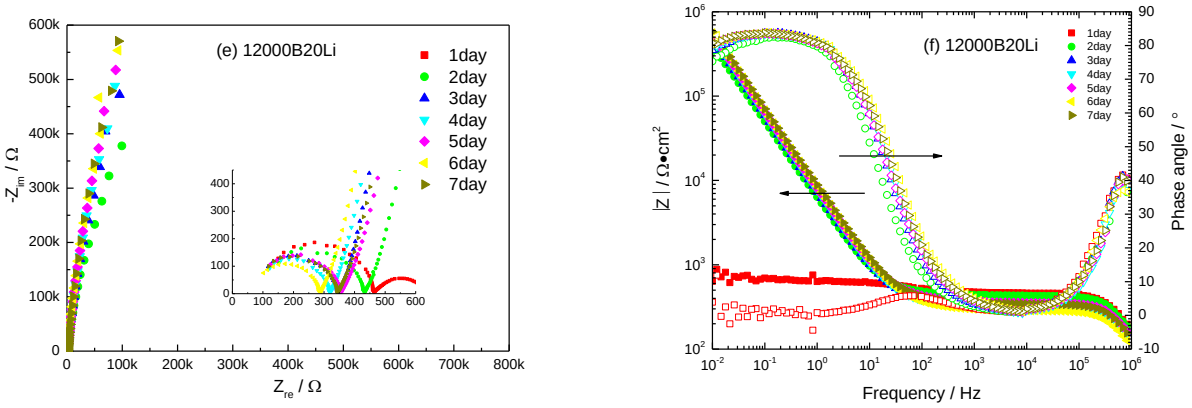

Figure 3. EIS (a, c, e) Nyquist and (b, d, f) Bode diagrams of SS316L measured at the OCP in various boric acid solutions at 50°C for 7 days. Insets show the low frequency results.

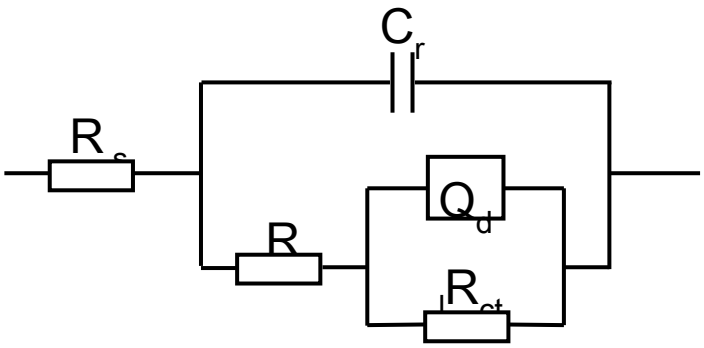

Figure 4. The equivalent electrical circuit used to emulate the impedance spectra for the double layer structure on stainless steel.

Previous papers [19-21] noted that the passive films on stainless steel have a double layer structure, and the inner layer is mainly formed by chromium oxide and the outer layer is mainly formed by iron-nickel oxide. Based on this structure, various types of fitting circuits were proposed [22, 23]. In this experiment, an improved two-layer structure of the circuit was tested evaluate the experimental EIS data, as shown in Fig. 4. R_s is the contact and the solution resistance, C_r is the capacitance of the passive film, R_r is resistance of the passive film and the corrosion products, R_{ct} is the charge transfer resistance., Q is the constant phase-angle elements of the electric double layer. Here, CPE has an impedance dispersion relation of $Q=1/Y_0(j\omega)^n$. If n=1, 0 or 1, the CPE represents a capacitance (C), a resistance (R) or an inductance (L), respectively.

ZSimpwin ™ 3.21 was employed to fit the experimental results with the circuit diagram. Typical fitting values for corrosion times of 1 day, 4 days and 7 days are listed in Table 2. The resistance of the solution decreased during the corrosion process for each solution. The resistance of the outer layer of the passive film changed at irregular intervals for the samples in different solutions. The resistance inner layer of the passive film increased during the corrosion process in every solution with boric acid. This means that immediately after immersion in boric acid, the inner layer of the

passive film on the stainless steel played a small role and had a small protective effect, and as time increased, this layer grew, resulting in a higher resistance. The capacitance of the outer layer of the passive film increased during the corrosion process.

Table 2. Parameter values obtained from the EIS data fitting.

		$R_s(\Omega)$	$C_r(F)$	$R_r(\Omega)$	Q_{dl} CPE	n	$R_{ct}(\Omega)$
(B)1200B2Li	day1	452.6	1.16E-09	641.5	4.72E-05	0.7575	4.69E+05
	day4	327.8	3.23E-09	389	2.07E-05	0.7574	2.55E+19
	day7	234.5	3.19E-09	312.6	1.65E-05	0.758	1.15E+20
(C)6000B10Li	day1	449.4	2.69E-09	421.4	5.62E-05	0.8205	3.87E+05
	day4	333.9	4.68E-06	736.4	2.41E-05	0.7976	5.44E+15
	day7	329.2	4.31E-06	855.8	2.17E-05	0.7998	1.00E+19
(D)12000B20Li	day1	422.3	6.69E-09	450.2	4.04E-04	0.7654	2.61E+4
	day4	348.7	2.10E-08	387.0	1.42E-05	0.8314	3.86E+16
	day7	260.4	1.35E-08	98.55	2.14E-05	0.9049	3.61E+18

After one day of corrosion, the $|Z|_{0.01Hz}$ and phase angle showed the same change as the other solution concentrations. Due to the anti-corrosion properties of SS316L, the passive film mainly inhibited the protective behaviours rather than the corrosion behaviours during this test. The corrosion resistance of the surface film mainly depends on the corrosion resistance of the inner passivation film[24-27]. The value of R_{ct} is much larger than that of R_r, which indicated that the corrosion protection ability of SS316L in various boric acid mainly depends on the inner layer. The value n of Q, which indicated the constant factor of phase-angle elements, played much closer to 1 indicating that the dispersion effect decreased. CPE value decreased with time, indicating that the inner passivation film is thicker and thicker, and accordingly, the resistance R_{ct} of the passive film is also larger and larger. The passive film of SS316L immersion in various boric acid solutions for 7 days resulted in a maximum CPE of 6000B10Li, indicating the thinnest oxide film and the weakest corrosion resistance.

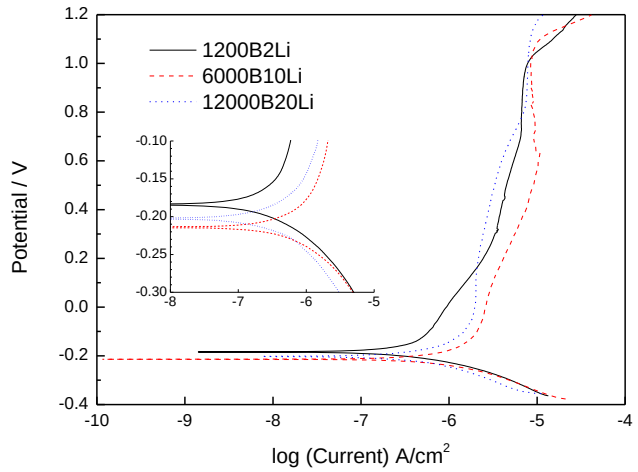

Figure 5. Potentiodynamic polarization curves of SS316L in various boric acid solutions at 50°C.

Table 3. Parameter values obtained from Tafel curves.

	Ecorr (mV)	Icorr (A.cm^{-2})	Ba (mv.dec^{-1})	Bc (mv.dec^{-1})
1200B2Li	-185	2.05E-07	250	65.75
6000B10Li	-215	8.66E-07	207.11	60.42
12000B20Li	-202	3.16E-07	206.33	44.9

Furthermore, potentiodynamic polarization was employed to investigate the corrosion behaviour of SS316L in various boric acid solutions at 50°C, as shown in Fig. 5 and in the inset showing the Tafel zone. The as-calculated Tafel data is listed in Table 3.

3.2. Morphologies and compositions of oxide films on stainless steel 316L

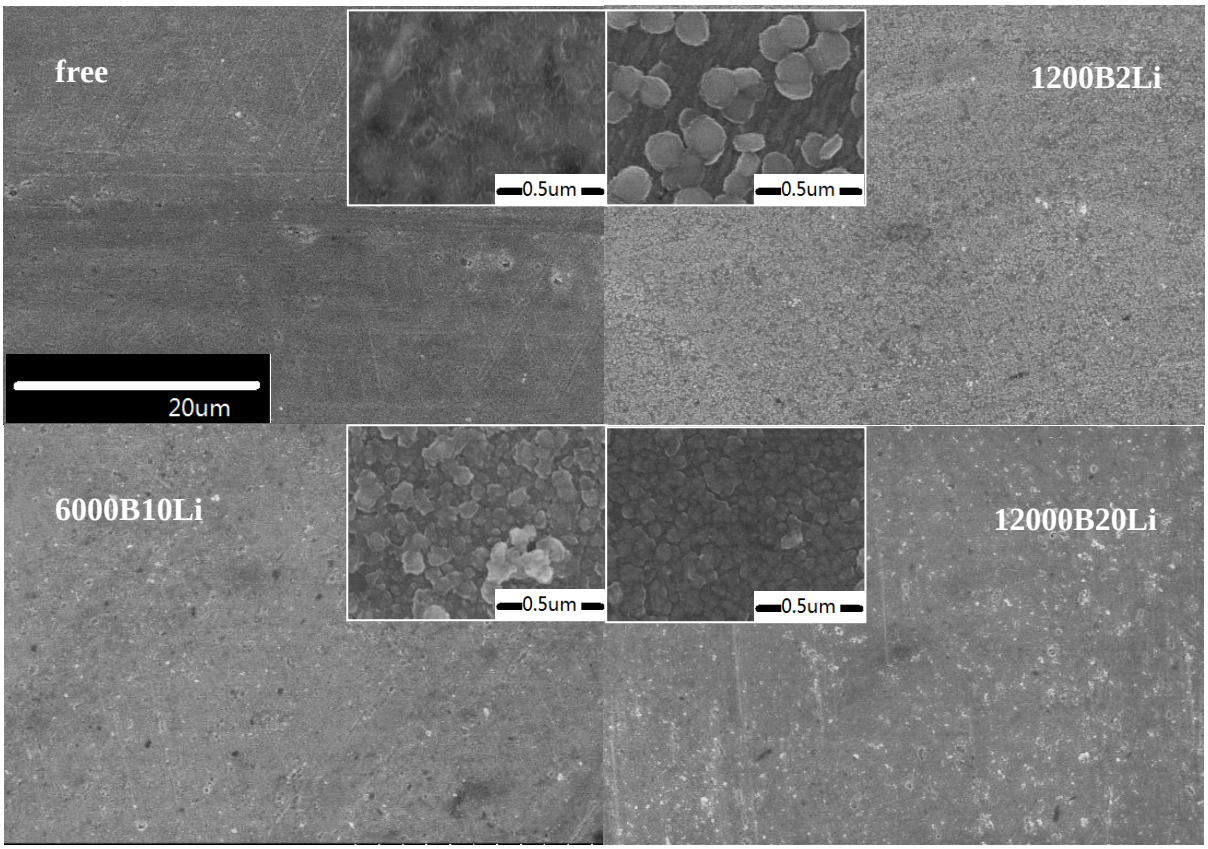

Figure 6. The SEM micrographs of SS316L after being corroded in various boric acid solutions for 7 days at 185°C.

Fig. 6 shows the SEM micrographs of the samples after corrosion at 185°C in various solutions. The inset pictures show the details. The main corrosion type of SS316L was general corrosion. There were significant differences between the boric-free solution and boric acid solutions. Many products were observed in the micrographs of the films formed in the boric acid solutions. Normally, passive films formed on stainless steel in boric acid buffered solutions should be somewhat protective. For

example, massive or acicular oxide formed on stainless steel surface during a long time immersion in high temperature and pressure water. With the composition of high temperature water changes, the morphologies of the protective film may also change[27-29]. In this experiment, the passive film formed in boric acid has particulate oxide, and as the acid concentration increases, the oxide particle size decreased. Also, there is pitting corrosion on the passive film of stainless steel in these boric acid solutions. The pitting corrosion is most severe in 600B10Li solution. It should highlight that, in neutral aqueous solution SS316L also involved pitting corrosion after 7 days immersion. This indicated that in the working condition of primary circuit of PWR, improperly concentrations of boric acid solution may play detrimental to the long term service of stainless steel.

The chemical compositions of the corrosion products after 7 days in boric acid solutions at 185°C were measured by EDS and are summarized in Table 4. It should be highlighted that every EDS scan was taken from an area scan of the whole field of view. The corrosion products in the boric acid solutions indicated almost the same concentrations. It should also be highlighted that the boric-free solution showed a much higher oxygen concentration than the others. Due to the lack of a buffer ability in the boric-free solution, the samples of SS316L corroded more heavily than the samples in the boric acid solutions, which is the same trend seen in the mass loss measurements.

Table 4. EDS results of the corrosion products of SS316L in boric acid solutions at 185°C

Composition (at. %)	Fe	Cr	Ni	O	Mo
boric-free	64.53	12.91	1.67	13.74	7.15
1200B2Li	71.05	14.21	1.86	5.30	7.58
6000B10Li	69.97	14.03	1.65	6.57	7.77
12000B20Li	70.48	14.32	1.80	5.61	7.79

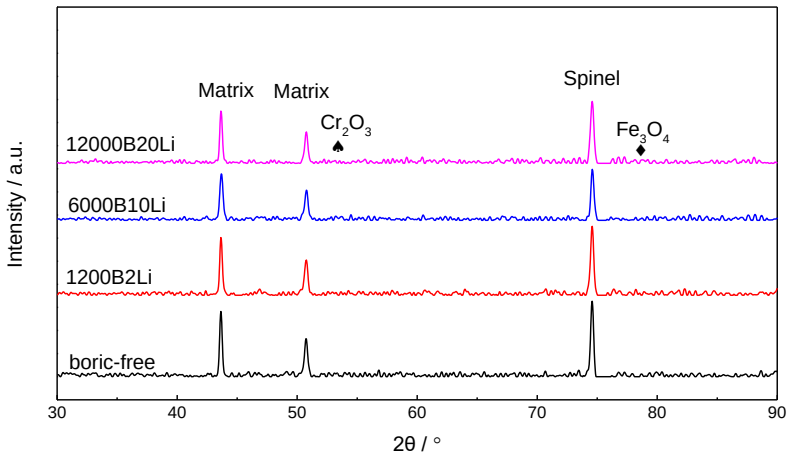

Figure 7. X-ray diffraction patterns of SS316 L with corrosion products after corrosion in various boric acid solutions for 7 days at 185°C

To clarify the composition of the oxide films on SS316L in boric acid solutions, XRD measurements were employed and are listed in Fig. 7. Though the surface of SS316L indicated different morphologies, the XRD patterns showed almost the same corrosion products. The surface primarily contained Fe, Ni, Cr and their oxides.

4. CONCLUSIONS

The effects of temperature and concentration on the corrosion behaviour of SS316L in boric acid with lithium hydroxide solutions simulating PWR primary circuit environments at 50-185°C were investigated. The following conclusions can be drawn from the test data. The corrosion rates of SS316L are very slow in boric acid solutions with both low and high concentrations. The electrochemical behaviour of SS316L corroded in a boric acid solution at 50°C shows that a passive layer formed on it. The morphologies of SS316L after corrosion in boric acid solution for 7 days at 185°C indicated a different degree of protective metal oxides formed on the surface.

ACKNOWLEDGEMENTS
This work was supported by the Fundamental Research Funds for the Central Universities.

References

1. J.M. Jenco, M. Bridges, Boric Acid Corrosion Guidebook, Revision 1, Managing Boric Acid Corrosion Issues at PWR Power Stations, *EPRI Report*, 2001.
2. A.S. O'neil and J.F. Hall, Boric Acid Corrosion of Carbon and Low Alloy Steel Pressure-boundary Components in PWRs, *EPRI Report*, NP-5985, 1988.
3. D.X. Chen, En-H. Han and X.Q. Wu, *Corros. Sci.*, 111 (2016) 518.
4. X.F. Xie, D. Ning, B. Chen, S.S. Lu and J. Sun, *Corros. Sci.*, 112 (2016) 576.
5. H.S. Klapper, J. Goellner, A. Burkert and A. Heyn, *Corros. Sci.*, 75 (2013) 239.
6. R.P. Matthews, R.D. Knusten, J.E. Westraadt and T. Couvant, *Corros. Sci.*, 125 (2017) 175.
7. P.D. Bilmes, C.L. Llorente, C.M. Méndez and C.A. Gervasi, *Corros. Sci.*, 51 (2009) 876.
8. C.A. Gervasi, C.M. Méndez, P.D. Bilmes and C.L. Llorente, *Mater. Chem. Phys.*, 126 (2011) 178.
9. A. Fattah-alhosseini, M.A. Golozar, A. Saatchi and K. Raeissi, *Corros. Sci.*, 52 (2010) 205.
10. E.C. Souza, S.M. Rossittib and J.M.D.A. Rollo, *Mater. Charact*., 61 (2010) 240.
11. L.C. Casteletti, F.A.P. Fernandes and G.E. Totten, *Heat Treatment*, 24 (2009) 25.
12. P.D. Bilmes, C.L. Llorente, C.M. Méndez and C.A. Gervasi, *Corros. Sci.*, 48 (2006) 3261.
13. M. Uemura, T. Yamamoto and K. Fushimi, *Corros. Sci.*, 51 (2009) 1554.
14. M.da.C. Belo, M. Walls, N.E. Hakiki, J. Corset, E. Picquenard, G. Sagon and D. Noël, *Corros. Sci.*, 40 (1998) 447.
15. M. Vankeerberghen, G. Weyns, S. Gavrilov, J. Henshaw and J. Deconinck, *J. Nucl. Mater.*, 385 (2009) 517.
16. S.S. Hwang, *J. Nucl. Mater.*, 443 (2013) 321.
17. F. Arjmand, L. Zhang and J. Wang, *Nucl. Eng. Des.*, 322 (2017) 215
18. M. Metikoš-Huković, R. Babić, Z. Grubač, Ž. Petrović and N. Lajçi, *Corros. Sci.*, 53 (2011) 2176
19. J.M. Bastidas, M.F. López, A.Gutiérrez and C.L. Torres, *Corros. Sci.*, 40 (1998) 431.
20. M.J. Carmezima, A.M. Simõesb, M.F. Montemorb and M. Da Cunha Belo, *Corros. Sci.*, 47 (2005) 581.

21. F.J. Pérez, A. Gutierrezb, M.F. López c, M.P. Hierroa and F. Pedraza, *Thin Solid Films*, 415 (2002) 258.
22. J. Hitzig, K. Jüttner, W.J. Lorenz and W. Paatsch, *J. Electrochem. Soc.*, 133 (1986) 887.
23. K. Jüttner, W.J. Lorenz and W. Paatsh, *Corros. Sci.*, 29 (1989) 279.
24. M. Zhang, H. Liu, S. Kr. Karn, J. Duan, F. Guan, X. Zhai, S. Zhao, K. Li and B. Hou, *Int. J. Electrochem. Sci.*, 12 (2017) 2315.
25. R. H. Tammam and A. M. Fekry, *Int. J. Electrochem. Sci.*, 12 (2017) 8991.
26. B. Stellwag, *Corros. Sci.*, 40 (1998) 337.
27. Q. Guo, Y. Li, J. Qian, H. Yu and C. Chen, *Int. J. Electrochem. Sci.*, 12 (2017) 8929.
28. K. Liang, Y. Xu, W. Wang, R. Shi, Y. Tan and S. Zhang, *Int. J. Electrochem. Sci*., 11 (2016) 10928.
29. D. Du, K. Chen, H. Lu, L. Zhang, X. Shi, X. Xu and P. L. Andresen, *Corros. Sci.*, 110 (2016) 134.